Journal of
Materials Chemistry C

Accepted Manuscript

This article can be cited before page numbers have been issued, to do this please use: S. Lei, H. fan, X. ren, J. fang, L. ma and Z. liu, *J. Mater. Chem. C*, 2017, DOI: 10.1039/C7TC00815E.

ROYAL SOCIETY OF CHEMISTRY

rsc.li/materials-c

View Article Online
DOI: 10.1039/C7TC00815E

Novel sintering and band gap engineering of $ZnTiO_3$ ceramics with excellent microwave dielectric properties

Shenhui Lei†, Huiqing Fan*†, Xiaohu Ren†, Jiawen Fang‡, Longtao Ma†, Zhiyong Liu†

† State Key Laboratory of Solidification Processing, School of Materials Science and Engineering, Northwestern Polytechnical University, Xi'an 710072, China

‡ Institute for Superconducting and Electronic Materials, University of Wollongong, NSW 2522, Australia

Abstract: The $ZnTiO_3$ ceramics with pure phase were successfully synthesized for the first time by solid state reaction method. Its synthesis temperature was higher than the phase transition temperature, wherein the ZnO nano particles acted as inhibitor to prevent the formation of secondary phase: Zn_2TiO_4, which was inevitable by conventional preparation methods. As the small nano ZnO regions dispersed in the ceramic grains, the bulk diffusion of Ti ions, the formation of nucleation centers and migration of phase boundaries were largely suppressed, indicating that nano ZnO was desirable for stabilizing $ZnTiO_3$ phase above the phase transition temperature. The R$\underline{3}$ (No. 148) space group of single phase were determined by the X-ray diffraction Rietveld analysis. X-ray photoelectron spectroscopy and photoluminescence emission spectrum were also carried out to investigate the electronic microstructure of obtained $ZnTiO_3$ phase. Finally, excellent microwave dielectric properties were achieved (ε_r ~31.5, $Q\times f$ ~59,800 GHz and τ_f~1.2 ppm/°C) with high sintering temperature (900-950 ^{o}C). Moreover, given its good chemical compatibility with Ag electrode, merits of easy scale-up, high-efficiency, low-cost and environmental benign, $ZnTiO_3$ is a promising candidate for LTCC applications. This work paves a great step towards the practical application.

* Corresponding author, Tel: +86-29-88494463, Fax: +86-29-88492642, E-mail: hqfan3@163.com，leishenhui@163.com.

View Article Online
DOI: 10.1039/C7TC00815E

1. Introduction

With the fast development of wireless communication industry, recent decades witness the booming development of microwave dielectric materials. A lot of works have been done to achieve microwave dielectric ceramics with low dielectric loss (high quality factor Q), appropriate dielectric permittivity ε_r (low response delay), and near-zero temperature coefficient of resonant frequency τ_f towards high-band microwave and millimeter range. Their wide applications have extended to a variety of wireless communication products, such as mobile telephones and base stations, global positioning systems (GPS), wireless local area networks (WLAN), Wi-Fi, RFID, and ZigBee communication systems[1-3]. Small size, low-cost, facile, and high performance have become the key issues in priority to apply to wireless communication devices. Along with the rapid development in communication technology, high-resolution and high-speed displays have become one of the growing trends. In this regards, candidate materials for such applications must have [1] proper high relative permittivity ε_r, [2] low dielectric loss or high quality factor Q (usually described in terms of a high $Q \times f$ product, where f is the resonant frequency), [3] near-zero temperature coefficient of resonant frequency (τ_f)[4,5]. Among them, perovskite oxide $ZnTiO_3$ has been applied to microwave devices, gas sensors (ethanol, NO, CO etc.), green chemistry catalyst or photo catalyst, UV-screening agent, photoluminescence, paint pigment and so on[6,7]. More than that, $ZnTiO_3$ based ceramic with excellent dielectric performances that can also reduce dimensions of the microwave low-power communication modules, has attracted more and more attention. The low sintering temperature makes it competitive for integrated smart system on a chip (SOC). It stands out as an important option material for the 4th generation cell phones offering the cell phone data speeds several times. However, it has to be noted that $ZnTiO_3$ ceramics are very sensitive both to temperature and synthetic processes. Generally, $ZnTiO_3$ ceramics will be thermally decomposed to secondary phase over 900 ^oC, which limits its performance in electronic devices, and hampers the prospects of commercialization in electronic devices[8,9]. On the other hand, low temperature co-fired ceramics (LTCC) have the advantages of incorporating

View Article Online
DOI: 10.1039/C7TC00815E

passive components into 3D microwave circuits and miniaturizing mobile devices. In the past few years, LTCC technology by using low cost electrodes (Ag, Cu, Al, *etc*.) for the benefits offered to the fabrication of miniature multilayer devices has received considerable attention[10,11]. Therefore, lowering the sintering temperature becomes unavoidable especially for mobile application, as the LTCC fabrication usually has to co-fire with Ag electrode at 950°C[12]. Thus, poor sintering stability and tight relationship with conventional process impedes its practical applications for $ZnTiO_3$ ceramics.

A series of works have been done in depth to obtain the pure $ZnTiO_3$ ceramic at required temperature with improved performance. For examples, $ZnTiO_3$ ceramics with various additives: ZnO-B_2O_3 glass, ZnO-SiO_2-B_2O_3 glass, B_2O_3 or B_2O_3-Li_2F[13-14] have manufactured at 900-930 ^oC, which inevitably introduce second phase with low Q value. Different dopants (Mg, Co etc.) brought into $ZnTiO_3$ ceramics[15] receive the same results due to unavoidable second phase. Other methods have also been tried to obtain pure $ZnTiO_3$ ceramics, such as molten salt synthesis (KCl, NaCl), self-propagating solution combustion synthesis, sol-gel method, hydrothermal method and solid state reaction method [16-19], yet the results are beyond satisfactory. Fundamental studies concerning the phase diagram and the characterization of ZnO-TiO_2 system are started by Dulin and Rase[20], Bartram and Slepetys[21]. It is reported that 3 kinds of compounds may exist in the ZnO-TiO_2 system, that is, Zn_2TiO_4, $ZnTiO_3$, and $Zn_2Ti_3O_8$. Despite this, the critical problems still are not solved for that $ZnTiO_3$ ceramics are very sensitive both to the temperature and the process, which turn out to be the bottleneck for the production of pure $ZnTiO_3$ based electronic devices.

To achieve this demand, in this study, low scanning rate precision DSC, quasi in-situ SEM and TEM analysis (rapid quenching method) are employed. Herein we find that (1) the phase evolution processes are governed by the bulk diffusion of Ti ions and the migration of phase boundaries. (2) The formation of second phase Zn_2TiO_4 follows the nucleation and growth mechanism. To the best of our knowledge, we obtain the pure $ZnTiO_3$ ceramics for the first time by an innovative use of

View Article Online
DOI: 10.1039/C7TC00815E

dispersive nano ZnO particles into a $ZnTiO_3$ matrix to avoid the formation of nucleation centers as well as to inhibit the migration of Ti ions. Thus, the phase transition reaction is successfully prevented. This simplified process provides a simple fabrication approach for low-cost microwave dielectric systems via standard solid state reaction method. Finally, pure $ZnTiO_3$ ceramics possess an ultra-low loss (or ultra-high quality factors, $Q \times f$ >40000 GHz) after cofiring with internal Ag electrodes in special patterns. Moreover, Rietveld analysis of X-ray diffraction patterns, XPS and PL spectrum have been conducted to understand their intrinsic dielectric properties. Its impressive microwave dielectric properties, good compatibility with Ag electrodes and excellent temperature stability, make the $ZnTiO_3$ ceramic an outstanding competitor for electronic communication devices.

2. Experimental Procedure

Pure $ZnTiO_3$ ceramics (ZnO-TiO_2), were prepared using the standard solid-state reaction processing[22] from mixed high-purity zinc oxide (ZnO), titanium dioxide (TiO_2) powders (≥99.8 wt%; Sinopharm Chemical Reagent Co., Ltd, China). To remove moisture retains, the TiO_2 powder were calcined at 600 °C for 2 h and cooling in dry. The stoichiometric ZnO, TiO_2 powders were mixed and ground together with ethanol medium for 10 h in a ball mill. The mixture were dried at 100 °C for 10 h, and then calcined at 750-850 °C for 3 h, as precursor powders. After sieved through a 200 μm sieve, the calcined powders were remilled with zirconia balls for 10 h in ethanol and got dried. Afterwards, the final powders were ground and pressed into disk pellets with a diameter of 12 mm and thickness of 2 or 6 mm at pressure of 300 MPa by cold isostatic press. Finally, the samples were sintered at 850-950 °C for 2-5h in air. In the second procedure, different constitutional $ZnTiO_3$ ceramics (ZnO-TiO_2), (y Zn:Ti=0.9, 1.0, 1.1, 1.2, 1.3; or amount of nano ZnO, y-1= 0, 0.1, 0.2, 0.3) were synthesized. The ZnO nanostructures were obtained via a novel economic one-step self-assembly synthesis using zinc nitrate hexahydrate, potassium hydroxide, cyclohexane-diamine-tetracetic acid (CDTA) and $C_6H_{12}N_4$ (HMAT).

The density of the sintered ceramics was calculated by Archimedes method with

View Article Online
DOI: 10.1039/C7TC00815E

distilled water. The crystalline phase of ceramics was examined with Powder X-ray diffraction data by using an automated diffractometer at room temperature (X'Pert PRO MPD, Philips, Eindhoven, Netherlands). The XRD data for Rietveld refinement was collected over the 2θ range of 10-130^{o} with a step of 0.02^{o} and a step time of 10 s, by using the GSAS-EXPGUI program[23,24]. The microstructure and surface morphologies of ceramics were investigated by a scanning electron microscopy (SEM; JSM-5610, JEOL, Japan Electron Co., Tokyo, Japan) with an applied voltage of 15 kV. Lattice images were observed by using high-resolution transmission electron microscopy (HRTEM; Tecnai F30G^{2}, FEI, Hillsboro, OR, USA) operated at 300 kV accelerating voltage. Raman scattering experiments were performed with an instrument (LabRAM HR800, Horiba JobinYvon, Lyon, France) in a backward scattering geometry (the exciting source was the 514.5 nm line from an argon ion laser). Differential scanning calorimetry as well as thermogravimetric analysis was also done to get the detail sintering information about the calcined ceramic powders (DIL 402, Netzsch, Freistaat Bayem, Germany). Chemical compositions and valence band spectra of the samples were analyzed using X-ray photoelectron spectroscopy (XPS, VG ESCALAB 220i-XL, Thermo Scientific, Waltham, MA, USA) with an AL Kα source (E=1486.6 eV). All binding energies were referenced to the C 1s peak (284.6 eV) arising from adventitious carbon. The optical absorbance spectra of as-synthesized products were performed in a UV-visible spectrophotometer (UV-vis DRS; Cary 500, Agilent, Santa Clara, CA, USA). Photoluminescence (PL) spectra was recorded at room temperature with a fluorescence spectrophotometer (F-4600, Hitachi Corp, Tokyo, Japan), excited by incident light of 325 nm.

All electrochemical tests were carried out using a three electrode cell where a platinum electrode and mercurous chloride electrode (3 mol L^{-1} KCl) acted as the counter electrode and reference electrode, respectively. The preparation procedure was according to the reference previously reported[25,26]. The work electrodes were prepared by screen-printed (area: 10 mm × 10 mm) on fluorine-doped tin oxide (FTO) glass substrates (FEC8, 8Ω per square, Xiangnan, China). Each screen-printed film was subsequently placed at room temperature for 10 min and then dried at 60 ^{o}C

View Article Online
DOI: 10.1039/C7TC00815E

for 30 min, and annealed at 350 ^{o}C for 1 hour to improve its adhesion.

To assess electrical property measurements, silver paste was painted on pellets as the electrodes and fired at 550 °C for 30 min. The dielectric properties were measured by a precision impedance analyzer (4294A, Agilent, Santa Clara, CA, USA) in the frequency ranging from 100 Hz to 1MHz with a heating rate of 2 °C • min^{-1}. The dielectric properties in the frequency range of 5-8 GHz were measured using network analyzer (8720ES, Agilent, Santa Clara, CA, USA) with the Hakki-Coleman dielectric resonator method[27]. The temperature coefficient of resonant frequency (τ_f) is defined as follow:

$$\tau_f = \frac{f_{80} - f_{20}}{60 \times f_{20}} (ppm/^{o}C) \quad (1)$$

where f_{20} and f_{80} represent the resonant frequencies at 20 °C and 80 °C, respectively.

3. Results and discussion

As the $ZnTiO_3$ ceramic is very sensitive to the temperature, it is calcined at variable temperatures (750-900 ^{o}C), and their corresponding final composition are shown in Fig. S1. (Supplemental informations). It is found that the low temperature phase $Zn_2Ti_3O_8$ is largely reduced after a long holding time (4-5 h) at a proper low presintering temperature (800 ^{o}C). Fig. S1(c) shows that the reaction of phase transition happened at 900 ^{o}C can be divided into 2 parts, and the former reaction reacts fast attributed to the constituent fluctuation caused by migration of Ti ions. This is evidenced by a steep slope in the DSC curve. It takes a longer time for the latter reaction to complete, as is related with the difficult and accumulating process in nucleation and growth of the new phase.

In Fig. 1(c-d) and Fig. 2, it also certifies that TiO_2 precipitate is very important in the phase transition from $ZnTiO_3$ to Zn_2TiO_4 (by rapid quenching methods), usually as the initial nucleation centers. We also find that the nucleation and growth of new phase are governed by bulk diffusion of Ti ions and migration of phase boundaries. Meantime, the formation of second phase Zn_2TiO_4 follows the nucleation and growth mechanism, and it takes a long time to finish the phase transition. This result makes a possible way to obtain the pure $ZnTiO_3$ phase by introducing in nano ZnO inhibitor

View Article Online
DOI: 10.1039/C7TC00815E

regions.

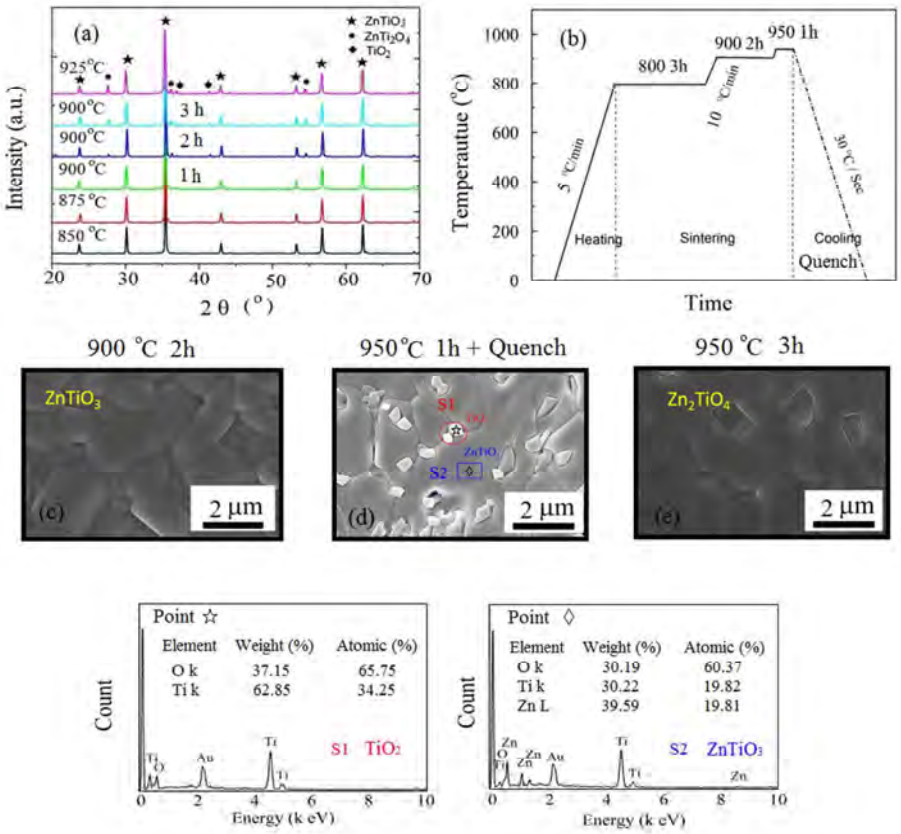

Fig. 1 The XRD and SEM analysis of $ZnTiO_3$ ceramic under different processing conditions. It reveals that the formation of Zn_2TiO_4 is time dependent and TiO_2 precipitate is the critical path in phase transition from $ZnTiO_3$ to Zn_2TiO_4.

On the other hand, the homogeneous ZnO nano particles with uniform size of 10-15 nm are successfully prepared via simple solution method, evidenced in the TEM images, and details are included in supplemental information. We successfully obtain the pure $ZnTiO_3$ phase by creatively introducing nano ZnO inhibitor regions. The involved mechanism is depicted in Fig. 2. The natural hexagonal structure of ZnO tend to form two different layers with opposite charges at the top and bottom surfaces of the primary hexagonal prism: O^- layer and Zn^+ layer, respectively. When the Ti ions pass through the layers with different charges, they are prone to be trapped by the O^- layer and react with the ZnO nano particles. The process can be described by the equation [$ZnO + TiO_2 \rightarrow ZnTiO_3$ (950 °C)]. As a result, the nucleation and

View Article Online
DOI: 10.1039/C7TC00815E

growth of secondary phase, as well as the bulk diffusion of Ti ions have been largely depressed[28-29]. Therefore, the single phase of $ZnTiO_3$ can be successfully kept above the phase transition temperature.

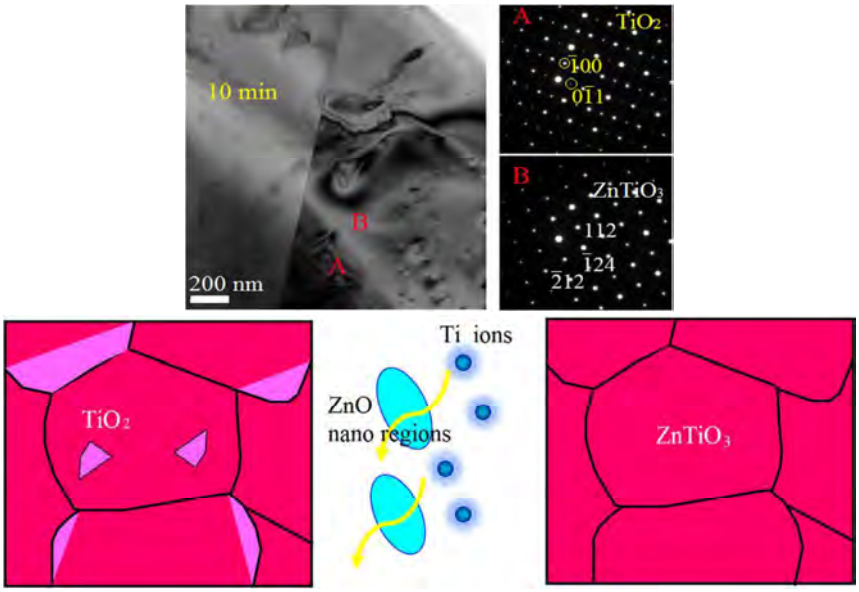

Fig. 2 The bright field images of the $ZnTiO_3$ ceramic sintered at 950 ^oC for 10 min based on quenching method. TiO_2 precipitate (A spot) and $ZnTiO_3$ ceramic matrix (B spot) are shown in the SEAD patterns. This find makes a possible way to obtain the pure $ZnTiO_3$ phase by introducing in nano ZnO inhibitor regions as exhibited.

It's worth mentioning that, for y-1=0.2～0.3, the pure $ZnTiO_3$ phase is evidenced according to the standard pattern of $ZnTiO_3$ phase (JCPDS #58-0547). As exhibited in Fig. 3, the ceramic with no nano ZnO buffer regions contains two main phases $ZnTiO_3$ and Zn_2TiO_4 (JCPDS #25-1164). SEM and Raman analysis demonstrate the feasibility of pure $ZnTiO_3$ phase just as the XRD. These two phases have different morphologies in ceramic grains; the white one correspond to $ZnTiO_3$ phase, and dark one is Zn_2TiO_4 phase, as shown in Fig 3(b). However, with addition of nano ZnO particles (y=1.2), this transition can successfully be held back. According to the literatures of hexagonal perovskites, the TiO_6 oxygen octahedron with O_h symmetry has 6 fundamental vibrations modes: symmetric stretching mode A_{1g}, asymmetric stretching mode E_g and F_{1u}, asymmetric bending mode F_{2u}, symmetric bending mode F_{2g} and inactive mode F_{2u}. The group theoretical considerations represent the 15

View Article Online
DOI: 10.1039/C7TC00815E

internal modes of oxygen octahedron[30,31] as $A_{1g}+ _{Eg} +2F_{1u}+F_{2g}+F_{2u}$. The vibration modes A_{1g}, E_g, $2F_{1u}$ and F_{2g} are Raman active and have been labeled in the Fig. 3(c), while F_{2u} is inactive. The symmetric stretching vibrations of the edge-connected octahedra are observed at about 730 cm^{-1}, which originate from the A_{1g} mode. The corner-connected octahedra observed at 610 cm^{-1} is corresponding to the E_g mode. The bands located at 300 cm^{-1} and 340 cm^{-1} originate from band F_{2g}, and the band at 450 cm^{-1} originates from F_{1u}. The bands located below 280 cm^{-1} (bands 1-6) are due to lattice modes. A clear assignment of these modes is not possible due to the fact that this region consists of complicated vibrations including translational and rotational modes of oxygen octahedral and metal-oxygen stretching modes. However, the appearance of these peaks indicates the phase transition is sensitive to the nano ZnO additive, and these peaks can be ascribed to the formation of secondary phase Zn_2TiO_4. The band 7 represents a statistical chance of ions different types occupying adjacent octahedral. (Zn^{2+} occupying the position of Ti^{4+}). It means that the vibration mode all shift toward the high-frequency direction (blue shift) and it can be ascribed to the increase of bond force that results in decreased vibration scope in the equilibrium position. In all, XRD, SEM and Raman analysis totally reveal a change in crystal structure with introduced nano ZnO. The outstanding properties (ultra-low loss, usually $Q\times f \geq$ 4,000GHz) are obtained in the pure $ZnTiO_3$ ceramics for y=1.2～1.22, with ε_r ~31.2, $Q\times f$ ~59,800 GHz and τ_f~1.5 ppm/°C shown in Tab. 1 (more details in the supplemental informations).

The key microwave dielectric parameters of the $ZnTiO_3$ based ceramics are summarized in Tab. 1. The ceramic with y-1=0.2～0.22 (nano ZnO) have excellent properties. As far as we know, they are the best among $ZnTiO_3$ ceramics reported, nearly two times as the related references. The dielectric permittivity ε_r (directly related to the electric capacitance), mechanical quality factor Q value (Q=1/tan δ, closely related to the crystal lattice energy, as a key parameter for the dielectric loss) and τ_f (the temperature stability) are all important parameters for many materials.

View Article Online
DOI: 10.1039/C7TC00815E

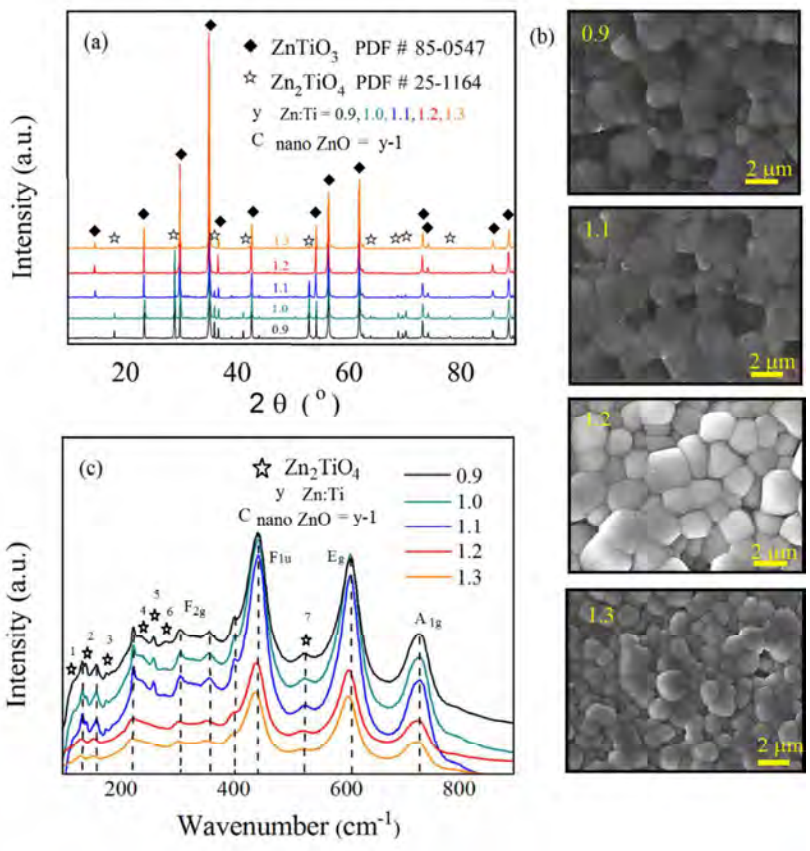

Fig. 3. The relationship between the amount if nano ZnO particles and the resulting $ZnTiO_3$ ceramics are carefully studied. (a) XRD patterns (b) SEM images and (c) Raman spectra of $ZnTiO_3$ ceramics with different y ratio, the amount of nano ZnO particles $C_{\text{nano ZnO}}$ is equivalent to (y-1) mol.

As shown in Fig. 4, the pure $ZnTiO_3$ phase also has been certificated by TEM analysis. Obviously, the microstructures become more homogeneous with increasing nano ZnO content. The selected electron diffraction pattern (SEAD) collected from crystal ceramic grain is assigned to $ZnTiO_3$ phase with [220] beam incidence. The HRTEM image of a single crystalline ceramic grain shows the [220] crystal orientation, and the (220) plane with spacing distance of about 0.3 nm in consistent with PDF card ($ZnTiO_3$, JPCDS #58-0547).The appearance of pure $ZnTiO_3$ phase can be explained by the inhibitor mechanism of nano ZnO shown in Fig. 2; hence, it is expected that the principle is also applicable to other materials encountering phase transition. As exhibited in Fig. 4, the dispersive ZnO nano regions can dissolve the TiO_2 precipitation, to form a pure $ZnTiO_3$ phase. [$ZnO + TiO_2 \rightarrow ZnTiO_3$ (950 °C)]

View Article Online
DOI: 10.1039/C7TC00815E

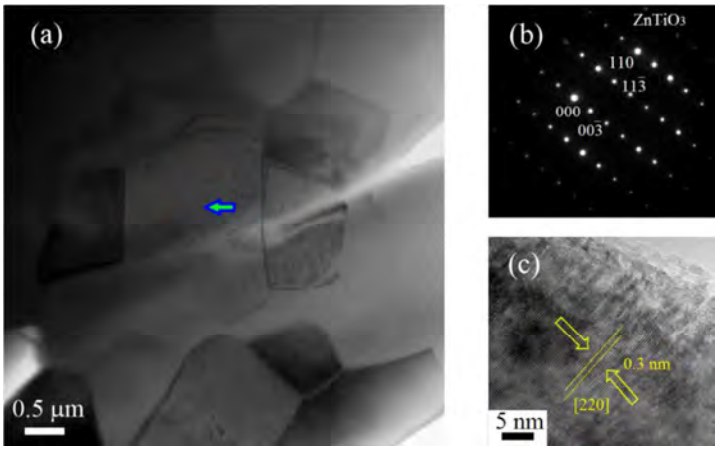

Fig.4 (a) TEM bright field images of the $ZnTiO_3$ ceramic sintered at 950 ^oC for 3 h, (b) the SEAD patterns for pure $ZnTiO_3$ phase, (c) the HR-TEM image for pure $ZnTiO_3$ phase. The arrow indicates the cloud-like dispersive nano ZnO regions in very small size.

To investigate the precise difference of electronic structure of the obtained $ZnTiO_3$ pure phase mentioned above, UV-vis absorption spectra and electrochemical Mott-Schottky plots are carried out (Fig. S7, supplemental informations). To further get the relative position of the valence band maximum and conduction band minimum for $ZnTiO_3$ as well as ZnO nano particles, their valence bands are also analyzed by XPS. The band gaps are calculated by the following equation[32]:

$$(\alpha h\nu)^{1/2} = A(h\nu - E_g) \qquad (2)$$

where α, ν, h and E_g denote the absorption coefficient light frequency, Planck constant and band gap, respectively. The valence band maximum and conduction band minimum for ZnO and $ZnTiO_3$ are analyzed by HR-XPS. As shown in Fig. 5, the valence band maximum of $ZnTiO_3$ is located at 2.83 eV. It reveals that ZnO has a higher valence band maximum than $ZnTiO_3$ by 0.06 eV. It is further confirmed by the results of band gap analysis in UV-vis diffuse reflectance spectra, PL (photoluminescence) spectra and flat band potential positioning (Fig. S4).

View Article Online
DOI: 10.1039/C7TC00815E

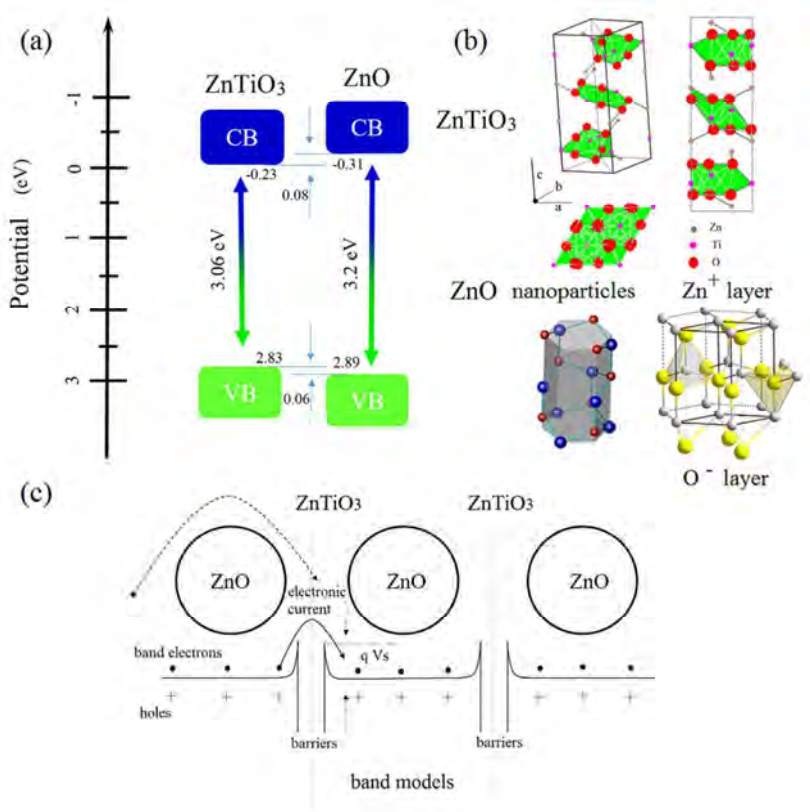

Fig.5 (a) Electronic band structure of $ZnTiO_3$ and ZnO. (b) Crystal structures of pure $ZnTiO_3$ phase and ZnO phase, respectively. $ZnTiO_3$ phase has a hexagonal structure in space group R$\underline{3}$ (No.148). (c) Band models for pure $ZnTiO_3$ ceramic with nano ZnO regions.

The position of the valence band maximum and conduction band maximum could also be roughly evaluated by following equation[33]:

$$E_{VBM} = \chi - E_e + 1/2E_g \qquad (3)$$

where E_{VBM} is the valence band maximum potential, χ is the Mulliken electronegativity of the constituent atoms in the semiconductor, E_g is the band gap, and E_e is the constant value of energy of free electrons on the hydrogen scale. Based upon these analyses, band alignments, including the valence band and conduction band of the pure $ZnTiO_3$ phase as well as ZnO nano particles are presented in Fig. 5.

The excellent performance of pure $ZnTiO_3$ phase can also be evidenced by the investigated electrochemical impedance spectra accompanying an interpretation according to an equivalent circuit model (Fig. 5c). Compared with the other reports on $ZnTiO_3$ materials via different methods (Tab. 1), the new synthesized $ZnTiO_3$ ceramic

View Article Online
DOI: 10.1039/C7TC00815E

in this work has an extraordinary low loss and very good temperature stability. To gain a thorough investigation of the reasons, impedance spectra are measured accompanying an interpretation of an equivalent circuit model, and the results are depicted in Fig. S8. The variable frequency impedance data are shown for measurements in N_2 and O_2. There are two well-defined Nyquist plots in high- and middle- frequency region, and these two arcs indicating that the material contains two principal electrical component: the ceramic grains and grain boundaries. The electron transfer resistance modelled with an equivalent circuit exhibits in the inset of Fig. S8. Given the impedance data in N_2 and O_2 at 300 ^{o}C, the natural impedance Z' are both larger for $ZnTiO_3$ ceramic and Zn_2TiO_4 ceramic in O_2 atmosphere compared with that in N_2. The Z' of O_2 samples is higher than N_2 samples (lower conductivity), suggesting that the n-type conductivity in N_2 is a dominating process and the required electrons are created through the oxygen loss process:

$$O_o^x \rightarrow V_o^{\bullet\bullet} + 2e' + \frac{1}{2}O_2 \qquad (4)$$

In O_2 atmosphere, the oxygen vacancies evolved are suppressed in the high temperature sintering process, and the ceramic grains become relatively more insulating.

$$V_o^{\bullet\bullet} + \frac{1}{2}O_2 \rightarrow O_O^x + 2h^{\bullet} \qquad (5)$$

The holes could be trapped by the electrons from the reduction of Ti ions, as a formula of $Ti^{3+} \leftrightarrow Ti^{4+}$. From the Fig. S8(e, f), the conductivity for $ZnTiO_3$ with $y_{Zn:Ti}$= 0.9-1.2 (or nano ZnO= *y-1*) have apparent reduction in the air (more insulating), and the sample with pure $ZnTiO_3$ phase (y=1.2) is not sensitive to the atmosphere O_2, N_2, and air, suggesting an extraordinary low loss or largely consumption of defect carriers. This phenomenon reveals that the grain controlling mechanism dominate the grow process of samples. Meanwhile, in the same atmosphere O_2 or N_2, Z' value of the $ZnTiO_3$ ceramic is nearly 4 times bigger than that of Zn_2TiO_4 ceramic (13.2 MΩ to 3.8 MΩ in O_2 and 1.2 MΩ to 0.26 MΩ in N_2), disclosing that it is more difficult for carrier transfer (i.e., electron and holes). The deep reason is explained in the band models part, Fig. 5(c). As the discrepancy in the band gaps between $ZnTiO_3$ and nano

View Article Online
DOI: 10.1039/C7TC00815E

ZnO, the energy barriers to electron/hole transfer are formed in the path. The barrier height can be estimated as qV_s, where the V_s is the difference in the conduction band (about 0.08 eV). The dispersive nano ZnO regions form a continuous group of barriers, similar to the series resistance effect. As a result, it induces a large reduction in the hole or electron transporting.

Thus, the highly strengthened properties are ascribed to the pure phase of materials and the optimized band structure resulting from the dispersive nano ZnO buffer regions.

Generally, the cofired temperature with Ag electrode is 950 °C. However, as the temperature of phase conversion is exactly in this range, it's conflicted with the demand for LTCC application. Finally, we test the temperature stability of the obtained pure $ZnTiO_3$ phase, and its compatibility with the Ag electrode for LTCC practical application. The Fig. 6(a, b) shows the SEM image and EDS line scan of the interface between Ag electrode and the $ZnTiO_3$ materials co-fired at 950 ˚C for 3 h. The results indicates the single pure $ZnTiO_3$ phase can be well preserved even after high temperature sintering process of 950 ˚C (above the phase transition temperature), still possessing excellent performance, ε_r~31.5, $Q\times f$ ~59,800 GHz and τ_f~1.2 ppm/°C. The Ag profile decreases sharply at the interface, indicating that Ag atoms do not diffuse into the ceramic during sintering. There is no sign of Zn, Ti in the Ag electrode, suggesting that no reaction occurred at the interface. The fracture surface image of the $ZnTiO_3$ material implies that there are no secondary phase formed in the sintering process or cracks/pores, and the microstructures of $ZnTiO_3$ materials are homogeneous. Since the pure $ZnTiO_3$ phase has good chemical compatibility with Ag, it constitutes a promising candidate for LTCC applications. Furthermore, the resulting pure $ZnTiO_3$ ceramics are mechanically stable and the synthetic method is novel because the highly productive $ZnTiO_3$ materials can be directly used to fabricate the chemical or electronic devices via a simple and low-cost process.

View Article Online
DOI: 10.1039/C7TC00815E

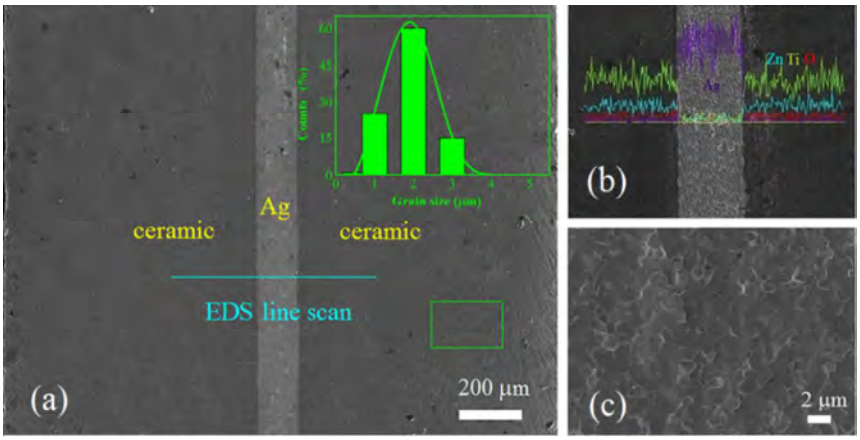

Fig. 6 the fractured surface of the $ZnTiO_3$ ceramic co-fired with Ag electrode at 950 ^oC for 3h. (a) FE-SEM image of the fracture section, (b) EDS line scanning result across the interface, (c) the dense fractured microstructure of $ZnTiO_3$ ceramic without secondary phase or pores. The inset shows the uniform size distribution of the ceramic grains.

4. Conclusions

We obtained a pure phase of $ZnTiO_3$ ceramic upon the phase transition temperature via the standard solid state reaction method for the first time; hereby the ZnO nano regions act as the inhibitor to prevent the formation of secondary phase: Zn_2TiO_4, which is inevitable by using the conventional preparation methods. It is certificated to have two dominant factors controlling the phase transition: the bulk diffusion of Ti ions and the migration of phase boundaries, which play important roles in nucleation and growth of the new phase. As the small nano ZnO buffer regions disperse in the ceramic grains, the bulk diffusion of Ti ions, the formation of nucleation centers and the migration of phase boundaries are largely suppressed. Thus the pure $ZnTiO_3$ phase can be preserved beyond the phase transition temperature. Excellent microwave dielectric performance of ε_r~31.5, $Q\times f$ ~59,800 GHz and τ_f~1.2 ppm/°C is obtained, and so far, the ultra-low loss is the highest performance in $ZnTiO_3$ materials. Since the pure $ZnTiO_3$ phase has good chemical compatibility with Ag electrode at a broad temperature form 900 to 950 ^oC, it constitutes a promising candidate for LTCC applications. Due to the merits of easy scale-up, high-efficiency, low-cost and environmental friendliness, the highly productive $ZnTiO_3$ materials

View Article Online
DOI: 10.1039/C7TC00815E

obtained by solid-state reaction can be directly used to fabricate the electronic devices via a simple and low-cost process. Overall, the analyses aforementioned can prove that the pure $ZnTiO_3$ ceramics with high performance will exhibit excellent characteristics for many using. It represents a great step towards the practical application of new electronic communication devices.

Acknowledgement
This work was supported by the National Natural Science Foundation (51672220), the 111 Program (B08040) of MOE, the National Defense Science Foundation (32102060303), and the Fundamental Research Funds for the Central Universities (3102014JGY01004) of China.

References
1 RJ. Cava, *J. Mater. Chem.* 2001, **11**, 54-62.
2 J. Guo, H.Z. Huo, A.L. Baker, M.T. Lanagan, E.R. Kupp, et al. *Angew. Chem. Int. Ed.* 2016, **55**, 1-6.
3 B. Liu, X.Q. Liu, X.M. Chen, *J. Mater. Chem. C* 2016, **4**, 1720-1726.
4 D. Zhou, D. Guo, W.B. Li, L.X. Pang, X. Yao, et al. *J. Mater. Chem. C* 2016, **4**, 5357-5362.
5 S.H. Lei, H.Q. Fan, W.N. Chen, Z.Y. Liu, M. Li, *J. Am. Ceram. Soc.* 2017, **100**, 235–246.
6 N.T. Nolan, M.K. Seery, S.C. Pillai. *Chem. Mater.*, 2011, **23**, 1496-1504.
7 J. Yang, J. Akbarzadeh, C. Maurer, H. Peterlik, U. Schubert, *J. Mater. Chem.* 2012, **22**, 24034.
8 H.T. Kim, S. H. Kim, S. Nahm, J.D. Byun, Y. Kim, *J. Am. Ceram. Soc.* 1999, **82**, 3043-3048.
9 Z.F. Fu, P. Liu, J.L. Ma, X.G. Zhao, H.W. Zhang, *J. Eur. Ceram. Soc.* 2016, **36**, 625–629.
10 T.W. Zhang, R.Z. Zuo, J. Zhang, *J. Am. Ceram. Soc.* 2016, **99**, 825-832.
11 B. Liu, L. Li, X.Q. Liu, X.M. Chen, *J. Mater. Chem. C* 2016, **4**, 4684-4691.
12 Di, Zhou, W.B. Li, H.H. Xi, L.X. Pang, G.S. Pang, *J. Mater. Chem. C* 2015, **3**, 2582-2588.
13 A. Chaouchi, M. Alouat, S.Marinel, S. D'Astorg, H. Bourahla, *Ceram. Int.* 2007, **22** 245-248.
14 H.T. Kim, M.T. Lanagan, *J. Am. Ceram. Soc.* 2003, **86**, 1874-1878.
15 A. Chaouchi, S. Marinel, M. Aliouat, S. d'Astrog, *J. Euro. Ceram. Soc.* 2007, **27**, 2561-2566.
16 Y.H. Yu, M. Xia, *Mater. Lett.* 2012, **77**, 10-12.
17 X. Liu, *Mater. Lett.* 2012, **80**, 69-71.
18 C.F. Shih, WM. Li, MM. Lin, KT. Hung, *J. Euro. Ceram. Soc.* **156**, 2009, E13-E17.

View Article Online
DOI: 10.1039/C7TC00815E

19 L. Bobowaka, A. Opasinska, A. Wypych, P. Wokcienchowski, *Mater. Chem. Phys.* 2012, **134**, 87-92.
20 F.H. Dulin, D.E. Rase, *J. Am. Ceram. Soc.* 1960, **43**, 125-131.
21 S.F. Bartram, R.A. Slepetys, *J. Am. Ceram. Soc.* 1961, **44**, 493-499.
22 K. Xu, J. Li, J.G. Wu, X.X. Zhang, D.Q. Xiao, et. al, *Adv. Mater.* 2016, **28**, 8519-8523.
23 A.C. Larson, R.B. Von Dreele, General Structure Analysis System (GSAS), LANL Report LAUR 86-748, Los Alamos National Laboratoty, Los AlAmos, NM, 2000.
24 B.H. ToBy, EXPGUI, a graphical user interface for GSAS. *J. Appl. Crystallogr.* 2001, **34**, 210-213.
25 J. Zhang, M. Zhang, R. Sun, X. Wang, *Angew. Chem., Int. Ed.*, 2012, **51**, 10145.
26 Liu, G.; Niu, P.; Sun, C.; Sean, C.; Chen, Z.; Lu, G.; Cheng, H. *J. Am. Chem. Soc.*, 2010, **132**, 1164.
27 BW. Hakki, PD. Coleman, *IEEE Trans. Microw. Theory Tech.* 1960, **8**, 402-410.
28 S. Farvid, P. Radovanovic, *J. Am. Chem. Soc.* 2012, **134**, 7015-7024.
29 S. Kumar, H. Mehdipour, K. Ostrikov, *Adv. Mater.* 2013, **25**, 69-74.
30 A. Damin, F.X.L. Xamena, C.B. Lamberti, C.M. Civalleri, A.ZW. Zecchina, *J. Phys. Chem. B* 2004, **108**, 1328-1336.
31 M.L. Moreira, EC. Paris, G.S. Nascimento, *Acta Mater.* 2009, **57**, 5174–5185.
32 Z. Liang, Q. Zhang, L. Jiang, G.Cao, *Energy Environ. Sci.,* 2015, **8**, 3442-3476.
33 Y. Hong, C. Tian, B. Jiang, A. Wu., Q. Zhang, G. Tian, H. Fu, *J. Mater. Chem. A,* 2013, **1**, 5700–5708.

View Article Online
DOI: 10.1039/C7TC00815E

Table. 1 Performance of $ZnTiO_3$ based materials using different preparation methods

Methods	Second phase	ε_r	$Q \times f$	τ_f	reference
Sol-gel	Zn_2TiO_4	19	35000	-55	[17]
hydrothermal	Zn_2TiO_4	25	-	18	[18]
solution	Zn_2TiO_4	26	32000	-90	[19]
Molten salt	Zn_2TiO_4	-	-	-	[16]
Solid state	Zn_2TiO_4	23	25000	15	[15]
Solid state	No	31.2	59800	1.5	This work

View Article Online
DOI: 10.1039/C7TC00815E

Graphic abstract